

---

# Variational Learning of Disentangled Representations

---

Yuli Slavutsky<sup>1\*</sup>

Ozgur Beker<sup>1,2\*</sup>

David Blei<sup>1,3</sup>

Bianca Dumitrescu<sup>1,2,3,4</sup>

<sup>1</sup>Department of Statistics, Columbia University, New York City, USA

<sup>2</sup>Irving Institute for Cancer Dynamics, Columbia University, New York City, USA

<sup>3</sup>Department of Computer Science, Columbia University, New York City, USA

<sup>4</sup>Columbia Stem Cell Initiative, Columbia University, New York City, USA

\*Equal contribution

## Abstract

Disentangled representations enable models to separate factors of variation that are shared across experimental conditions from those that are condition-specific. This separation is essential in domains such as biomedical data analysis, where generalization to new treatments, patients, or species depends on isolating stable biological signals from context-dependent effects. While extensions of the variational autoencoder (VAE) framework have been proposed to address this problem, they frequently suffer from leakage between latent representations, limiting their ability to generalize to unseen conditions. Here, we introduce DISCoVeR, a new variational framework that explicitly separates condition-invariant and condition-specific factors. DISCoVeR integrates three key components: (i) a dual-latent architecture that models shared and specific factors separately; (ii) two parallel reconstructions that ensure both representations remain informative; and (iii) a novel max-min objective that encourages clean separation without relying on hand-crafted priors, while making only minimal assumptions. Theoretically, we show that this objective maximizes data likelihood while promoting disentanglement, and that it admits a unique equilibrium. Empirically, we demonstrate that DISCoVeR achieves improved disentanglement on synthetic datasets, natural images, and single-cell RNA-seq data. Together, these results establish DISCoVeR as a principled approach for learning disentangled representations in multi-condition settings.

## 1 Introduction

Neural network-based models have shown impressive success in learning informative representations of complex data, and are increasingly used in scenarios where each data point  $x \in \mathcal{X} \subseteq \mathbb{R}^d$  is associated with a condition label  $y \in 1, \dots, K$ . In biological applications, for example, the condition may correspond to a treatment, patient, or species. In biological contexts, for instance, the condition might reflect a treatment, a patient, or a species. The learned representations often support downstream tasks such as domain adaptation and transfer learning (e.g., Pan et al. [2010]), enabling models to generalize from observed conditions to new, related ones. This requires learning disentangled data

representations that separate components of  $x$  shared across all conditions from those specific to a given condition  $y$ .

In recent years, generative models have emerged as a powerful class of methods for representation learning, thanks to their ability to model complex data distributions and capture underlying latent structure. Prominent examples include Generative Adversarial Networks (GANs) [Goodfellow et al., 2020], Variational Autoencoders (VAEs) [Kingma and Welling, 2014], and diffusion models [Sohl-Dickstein et al., 2015, Ho et al., 2020]. Among these, VAEs and their extensions have become particularly prominent in applications involving transfer learning and domain adaptation [Akrami et al., 2020, Lovrić et al., 2021, Godinez et al., 2022, Zhang et al., 2023], due to their principled probabilistic formulation and their ability to represent uncertainty in learned features.

Several recent VAE-based approaches have been proposed to integrate data from multiple conditions or sources [Xu et al., 2021, Lotfollahi et al., 2019, Boyeau et al., 2022]. However, only few explicitly aim to disentangle shared from condition-specific components [Sohn et al., 2015, Klys et al., 2018, Joy et al., 2020]. While these methods offer notable improvements in disentanglement, they either depend on carefully crafted priors, difficult to specify in high-dimensional complex settings like single-cell genomics, or fail to achieve a clean separation, limiting their utility in applications that demand robust generalization across conditions.

In this work, we propose a new framework for learning *disentangled representations in multi-condition datasets*. Our contributions are as follows: (i) We propose a new method based on two distinct reconstruction objectives combined with adversarial learning. Unlike prior approaches, our framework minimizes reliance on restrictive priors or handcrafted components, relying less restrictive assumptions. (ii) We formulate the task of learning disentangled representations as max-min optimization problem, derive a corresponding objective and give theoretical guarantees for the equilibrium of this objective. (iii) Through experiments on synthetic benchmarks and real-world datasets in computer vision and single-cell biology, we show that our approach consistently achieves better disentanglement of shared and condition-specific structure compared to existing methods.

## 2 DISCoVeR: DISentangling COMmon and Variant Representations

For the task of learning disentangled representations from multi-condition data, we consider a dataset  $\mathcal{D} = \{(x_i, y_i)\}_{i=1}^n$  consisting of inputs  $x_i \in \mathcal{X} \subseteq \mathbb{R}^d$  collected from associated condition labels  $y_i \in 1, \dots, K$ . We assume that for each class  $k$ , corresponding to a study or experimental condition, and that the associated subset  $\mathcal{D}_k := \{x_i : y_i = k\}$  consists of i.i.d. samples drawn from a class-conditional distribution  $p(x|y = k)$ .

### 2.1 Model assumptions

We assume that the data is generated by latent variables  $z$  and  $w$ , such that the joint distribution  $p(x, y, z, w)$  factorizes according to the probabilistic graphical model illustrated in Figure 1a, i.e.,

$$p(x, y, z, w) = p(y)p(w | y)p(z)p(x | z, w). \tag{1}$$

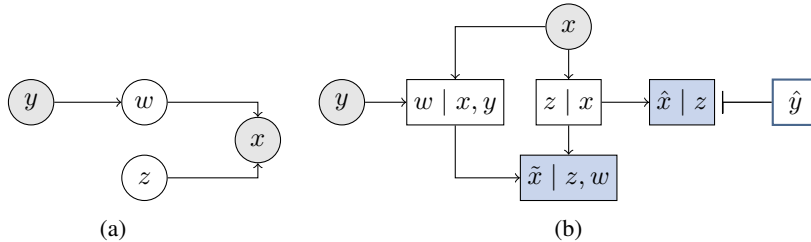


Figure 1: Graphical overview of our model. (a) Probabilistic graphical model: gray circles denote observed variables, white show latent variables. (b) Encoder-decoder architecture: the inhibition arrow from  $\hat{y}$  to  $\hat{x}$  corresponds to the adversarial component.

This model encodes two key conditional independence assumptions:

1. *Latent variable conditional independence:* Given the condition  $y$ , the latent representations  $z$  and  $w$  are conditionally independent:  $z \perp w \mid y$ .
2. *Sufficiency of the shared latent representation:* The input  $x$  is conditionally independent of the condition  $y$  given  $w$ :  $x \perp y \mid w$ .

However, note that in this model,  $z$  and  $w$  are no longer independent if conditioned also on  $x$ , that is,  $z \not\perp w \mid x, y$ .

## 2.2 Target posterior structure

In our model, the observed data  $x$  is generated from two latent variables,  $z$  and  $w$ . The marginal distribution of  $z$  is independent of the condition label  $y$ , making  $z$  *condition-invariant*, whereas  $w$  depends on  $y$  and is therefore *condition-aware*. Our goal is to learn probabilistic data representations such that the marginal distributions of  $z$  and  $w$  preserve the structure  $z \perp y$  and  $w \not\perp y$ , and therefore yield *disentangled representations*. For this, we approximate the joint posterior  $p_{z,w|x,y}$  via variational inference, enforcing that  $z$  remains independent of  $y$ , while  $w$  retains dependence on  $y$ . Our approach follows the empirical Bayes paradigm [Robbins, 1956], and in particular aligns with the principles of  $f$ -modeling introduced by Efron [2014], where the prior structure is inferred from the data to ensure consistency with observed marginals.

Ideally we would approximate the true posterior  $p_{z,w|x,y}$  with a variational distribution  $q_{z,w|x,y}$ . However, even under simple variational families such as multivariate Gaussians, capturing dependencies between  $z$  and  $w$  requires modeling a full covariance structure, which becomes computationally intractable in high dimensions. To mitigate this, we approximate the posterior  $p_{z,w|x,y}$  with a factorized variational distribution  $q_{z|x} q_{w|x,y}$ .

Our variational approximation is guided by two complementary objectives: (i)  $q_{z|x}$  closely approximating the marginal posterior  $p_{z|x}$ ; and (ii) the product  $q_{z|x} q_{w|x,y}$  closely approximating the true posterior  $p_{z,w|x,y}$ . Formally, given variational families<sup>1</sup>  $\mathcal{Q}_z$  and  $\mathcal{Q}_w$  we seek to find  $q_{z|x}^* \in \mathcal{Q}_z$  and  $q_{w|x,y}^* \in \mathcal{Q}_w$  that minimize the following sum of Kullback-Leibler (KL) divergences:

$$q_{z|x}^*, q_{w|x,y}^* = \arg \min_{\substack{q_{z|x} \in \mathcal{Q}_z \\ q_{w|x,y} \in \mathcal{Q}_w}} \text{D}_{\text{KL}}(q_{z|x} \parallel p_{z|x}) + \text{D}_{\text{KL}}(q_{z|x} q_{w|x,y} \parallel p_{z,w|x,y}). \quad (2)$$

## 2.3 Optimization objective

Direct computation of the KL divergences in Equation 2 is intractable. Therefore, we introduce a surrogate objective composed of three terms, two of which are evidence lower bound (ELBO) terms that minimize the sum of KL divergences without requiring their direct evaluation, and an additional adversarial term.

The corresponding ELBO objective to minimize  $\text{D}_{\text{KL}}(q_{z|x} \parallel p_{z|x})$  is

$$\mathcal{L}_z(q_{z|x}, p; x) := \mathbb{E}_{q_{z|x}} [\log p(x | z)] - \text{D}_{\text{KL}}(q_{z|x} \parallel p_z), \quad (3)$$

and the ELBO objective for the second KL term,  $\text{D}_{\text{KL}}(q_{z|x} q_{w|x,y} \parallel p_{z,w|x,y})$ , is given by

$$\mathcal{L}_w(q_{w|x,y}, p; x, y) := \mathbb{E}_{q_{z|x}} [\mathbb{E}_{q_{w|x,y}} [\log(p(x|z, w))]] - \text{D}_{\text{KL}}(q_{z|x} \parallel p_z) - \text{D}_{\text{KL}}(q_{w|x,y} \parallel p_{w|y}). \quad (4)$$

Note that  $\mathcal{L}_w(q_{w|x,y}, p; x, y)$  is the ELBO objective that corresponds to a factorized posterior  $q_{z|x} q_{w|x,y}$ . In Proposition 2.1 we examine the gap between this objective, and an ELBO term corresponding to a full variational posterior  $q_{z,w|x,y}$ . This can be interpreted as the cost of enforcing a condition-invariant latent representation, specifically, constraining  $z$  to depend only on  $x$ .

**Proposition 2.1.** *For random variables  $x, y, z, w$  following the graphical model in Figure 1a,*

$$\text{ELBO}(q, p; x, y) - \mathcal{L}_w(q_{w|x,y}, p; x, y) = \text{D}_{\text{KL}}(q_{z|x} \parallel p_{z|w,x,y}).$$

where  $\text{ELBO}(q, p; x, y) := \log p(x | y) - \text{D}_{\text{KL}}(q_{w|x,y} \parallel p_{w|x,y})$ .

<sup>1</sup>Here we consider general families and specify our concrete choices in Section 2.4.

The proof is provided in Appendix B.1.

Note that a full definition of the objectives in Equations 3 and 4 requires the specification of corresponding prior distributions, namely  $p_z$  and  $p_{w|y}$ . We defer their definitions to Section 2.4.

The ELBO objective in Equation 4 is defined over the conditional log-likelihood  $\log p(x | y)$ , and requires the addition of  $\log p(y)$  to correspond to the log-marginal likelihood  $\log p(x, y)$ . However, since  $\log p(y)$  does not depend on the variational distributions, including it in the objective has no effect on optimization. Still, we wish to ensure that the implicit marginal over  $y$ —as inferred from the latent representations, matches the true marginal  $p(y)$ . To this end, we introduce an auxiliary classifier  $g(y | z)$  as a form of posterior regularization [Ganchev et al., 2010]. This classifier captures the residual predictive signal about  $y$  contained in  $z$ , and is trained via the expected negative log-likelihood  $-\mathbb{E}_{q(z|x)} \log g(y | z)$ . If  $z$  is indeed independent of  $y$ , then  $g(y | z)$  will approximate the marginal distribution  $p(y)$ . By penalizing deviations from this behavior, we enforce the structural constraint  $z \perp y$  in the learned representation.

Note that for this term to effectively encourage  $q_{z|x}$  to discard condition-specific information, the classifier  $g_{y|z} \in \mathcal{G}$  must be optimized separately from the the rest of the model. This prevents degenerate solutions in which the third term is minimized without truly removing information about  $y$  from  $z$ , for example, by collapsing  $g$  to always predict a constant output, regardless of  $z$ .

Combining the three terms above, we define the objective

$$\mathcal{L}(q_{z|x}, q_{w|x,y}, g_{y|z}; x, y) = \mathcal{L}_z(q_{z|x}, p; x) + \mathcal{L}_w(q_{w|x,y}, p; x, y) - \mathbb{E}_{q_{z|x}} \log g(y | z), \quad (5)$$

which can be explicitly expressed as

$$\begin{aligned} \mathcal{L}(q_{z|x}, q_{w|x,y}, g_{y|z}; x, y) := & \mathbb{E}_{q_{z|x}} [\log p(x | z)] + \mathbb{E}_{q_{z|x}} [\mathbb{E}_{q_{w|x,y}} [\log p(x | z, w)]] \\ & - \mathbb{E}_{q_{z|x}} [\log g(y | z)] - 2 \text{D}_{\text{KL}}(q_{z|x} \| p_z) - \text{D}_{\text{KL}}(q_{w|x,y} \| p_{w|y}). \end{aligned} \quad (6)$$

Finally, to enable flexible trade-offs between reconstruction expressiveness and disentanglement, we introduce weighting terms  $\alpha = (\alpha_1, \alpha_2)$  into the objective following the motivation of  $\beta$ -VAEs [Higgins et al., 2017]:

$$\begin{aligned} \mathcal{L}_\alpha(q_{z|x}, q_{w|x,y}, g_{y|z}; x, y) := & \mathbb{E}_{q_{z|x}} [\log p(x | z)] + \mathbb{E}_{q_{z|x}} [\mathbb{E}_{q_{w|x,y}} [\log p(x | z, w)]] \\ & - \mathbb{E}_{q_{z|x}} \log g(y | z) - \alpha_1 \text{D}_{\text{KL}}(q_{z|x} \| p_z) - \alpha_2 \text{D}_{\text{KL}}(q_{w|x,y} \| p_{w|y}). \end{aligned} \quad (7)$$

Accordingly, the mean weighted objective is suitable for max-min optimization of the form:

$$\max_{q_{z|x} \in \mathcal{Q}_z} \max_{q_{w|x,y} \in \mathcal{Q}_w} \min_{g_{y|z} \in \mathcal{G}} \mathbb{E}_{p_{x,y}} [\mathcal{L}_\alpha(q_{z|x}, q_{w|x,y}, g_{y|z}; x, y)]. \quad (8)$$

## 2.4 Latent prior models and variational approximations

**Prior specification** We place a standard normal prior over the condition-invariant latent variable,  $p_z = \mathcal{N}(0, I)$ , which reflects a non-informative prior belief over its values.

For the condition-aware latent variable  $w$ , we define a class-conditional Gaussian prior  $p_{w|y}$ . As a simple specification, we model  $z$  and  $w$  to be of the same dimension, and specify

$$p(w | y = k) = \mathcal{N}(\mu_k, I) \quad (9)$$

$$\mu_k := \mathbb{E}_{p_{x|y=k}} [\mathbb{E}_{q_{z|x}} [z]]. \quad (10)$$

Here  $\mu_k$  is the mean of the inferred latent representations  $z$  within each class. Similarly, for different dimensions of  $z$  and  $w$  the mean aggregation can be replaced with a neural network that maps the inferred representations  $z$  for each class to the parameters of the Gaussian prior.

This specification induces a coupling between the two latent variables through the data distribution. Aligning  $p_{w|y}$  with the class-wise expectations of the invariant variable, further encourages  $q_{z|x}$  to encode informative representations, since capturing the shared structures will now not only increase  $\mathcal{L}_z(q_{z|x}, p; x)$ , but also decrease  $\text{D}_{\text{KL}}(q_{w|x,y} \| p_{w|y})$ , and thus increase  $\mathcal{L}_w(q_{w|x,y}, p; x, y)$ .

Importantly, for a truly condition-agnostic  $q_{z|x}$ , the conditional expectations  $\mu_k$  will collapse to a shared mean  $\mu := \mathbb{E}_{p_x} [\mathbb{E}_{q_{z|x}} [z]]$ . In this case  $p_{w|y}$  becomes a shared prior across classes, centered at a meaningful point in the latent space, rather than an uninformative one.

As the following proposition establishes, this anchoring of the prior  $p_{w|y}$  in the variational distribution  $q_{z|x}$  preserves the convex–concave structure of the objective, ensuring that the resulting max-min problem has a unique optimal solution.

**Proposition 2.2.** *Let  $\mathcal{Q}_z$  and  $\mathcal{Q}_w$  be convex parametric families of variational distributions over  $z$  and  $w$ , respectively, and let  $\mathcal{G}$  denote a convex set of classifiers such that  $g(x) \in [0, 1]$  for all  $g \in \mathcal{G}$ . Assume the latent priors are given by  $z \sim p(z)$  and  $p(w|y) = \mathcal{N}(\mu_y, I)$ , where  $p(z)$  is a continuous strictly positive distribution, and  $\mu_y = \mathbb{E}_{p_{x|y}} [\mathbb{E}_{q_{z|x}} [z]]$ . Then, under standard regularity conditions (see Appendix B.2.1), there exists a unique saddle point:*

$$\left( q_{z|x}^*, q_{w|x,y}^*, g_{y|z}^* \right) = \max_{q_{z|x} \in \mathcal{Q}_z} \max_{q_{w|x,y} \in \mathcal{Q}_w} \min_{g_{y|z} \in \mathcal{G}} \mathcal{L}(q_{z|x}, q_{w|x,y}, g_{y|z}).$$

The proof is provided in Appendix B.2.2.

**Specification of variational families** We set both variational families  $\mathcal{Q}_z$  and  $\mathcal{Q}_w$  as  $d$ -dimensional Gaussian distributions with diagonal covariance matrices. Accordingly, each variational distribution is parameterized by a mean vector  $\mu \in \mathbb{R}^d$  and a vector of variances  $\sigma^2 \in \mathbb{R}_+^d$  corresponding to the diagonal of the covariance matrix, yielding  $\theta = (\mu, \sigma^2)$ .

### 3 Encoder-decoder model

In order to optimize the objective in Equation 8 with respect to  $q_{z|x}$ ,  $q_{w|x,y}$  and  $g_{y|z}$  over the dataset  $\mathcal{D}$ , we introduce an encoder-decoder framework (for illustration see Figure 1b) in which two separate reconstructions of  $x$  are generated: one, denoted  $\hat{x} \sim p_{x|z}$ , where  $z$  is sampled from the condition-invariant posterior  $q_{z|x}$ , and the other, denoted  $\tilde{x} \sim p_{x|z,w}$ , where in addition,  $w$  is sampled from the condition-aware posterior  $q_{w|x,y}$ . The corresponding algorithm is summarized in Algorithm 1.

**Condition agnostic representation** An input  $x \in \mathcal{X}$  is mapped to the variational parameters  $\theta_z = (\mu_z, \sigma_z^2)$  by an encoder neural network  $f_\phi^z : \mathcal{X} \rightarrow \mathbb{R}^d \times \mathbb{R}_+^d$  parametrized by weights  $\phi$ . A latent encoding  $z \sim q_{\theta_z}$  is then sampled and mapped to a reconstruction  $\hat{x}$  via a decoder neural network  $h_\psi^z : \mathbb{R}^d \rightarrow \mathcal{X}$  parametrized by weights  $\psi$ .

**Adversarial classifier** To avoid constructing a complex classifier directly from  $z$  to  $y$ , we leverage the reconstruction  $\hat{x}$  from  $z$ . As a proxy for  $g(y|z)$ , we instead predict  $y$  from  $\hat{x}$ , allowing the use of a simple logistic regression on  $\hat{x}$ . Therefore, we define the adversarial classifier as a multinomial logistic regression  $g_\beta : \mathcal{X} \rightarrow [0, 1]^K$ , parametrized by class-specific weight vectors  $\beta = \{\beta_k\}_{k=1}^K$ .

While, from an information-theoretic perspective, this substitution weakens the estimation of the cross-entropy term  $-\mathbb{E}_{q_{z|x}} \log g(y|z)$ , since by the data processing inequality,  $\hat{x}$  can contain at most the information present in  $z$ , we observed this to be often preferable from an optimization perspective. Predicting  $y$  from  $\hat{x}$  helps reduce the variance introduced by sampling  $z \sim q_{\theta_z}$ , and thus acts as a form of regularization that prevents  $q_{\theta_z}$  from overfitting to noisy penalties produced by the classifier.

**Condition aware representation** A labeled input pair  $(x, y) \in \mathcal{X} \times \{1, \dots, K\}$  is mapped to the parameters  $\theta_w = (\mu_w, \sigma_w^2)$  using an encoder neural network  $f_\rho^w : \mathcal{X} \times \{1, \dots, K\} \rightarrow \mathbb{R}^d \times \mathbb{R}_+^d$  parametrized by weights  $\rho$ . A sample  $w \sim q_{\theta_w}$  is then drawn, and the pair  $(z, w)$  is mapped to a reconstruction  $\tilde{x}$  via a decoder neural-network  $h_\eta^{z,w} : \mathbb{R}^d \rightarrow \mathcal{X}$ , parametrized by weights  $\eta$ . To compute the prior  $p_{w|y}$ , we estimate the class-specific mean as  $\hat{\mu}_k := \frac{1}{n_k} \sum_{i:y_i=k} z_i$  where each  $z_i \sim p(z|x_i)$  is sampled from the encoder given an input  $x_i$  with label  $y_i = k$ , and  $n_k$  is the number of training points with the label  $y = k$ .

In practice, following standard approaches in VAE-based models, we make two approximations: (i) we use a single-sample Monte Carlo estimate to approximate the expectations in Equation 8, and (ii) instead of directly sampling from  $q_\theta$ , we employ the reparameterization trick to enable differentiable sampling. Specifically, we sample  $\epsilon \sim \mathcal{N}(0, I)$  and obtain a sample from  $q_\theta$  by applying a deterministic transformation of  $\epsilon$  based on the variational parameters  $\theta$ .

---

**Algorithm 1**

---

- 1: **Input:** Data  $\mathcal{D} = \{x_{1:n}, y_{1:n}\}$ , number of training iterations  $J$ , initial parameters  $\phi^{(0)}, \psi^{(0)}, \rho^{(0)}, \eta^{(0)}, \beta^{(0)}$ , learning rates  $\gamma_1, \gamma_2$ , weighting terms  $\alpha = (\alpha_1, \alpha_2)$
- 2: **for**  $1 \leq j \leq J$  **do**
- 3:   Compute  $\theta_z = f_{\phi^z}^z(x)$  and  $\theta_w = f_{\rho^{(j-1)}}^w(x, y)$
- 4:   Sample condition invariant and aware latent variables  $z \sim q_{\theta_z}$  and  $w \sim w_{\theta_w}$
- 5:   Compute reconstructions  $\hat{x} = h_{\psi^{(j-1)}}^z(z)$  and  $\tilde{x} = h_{\eta^{(j-1)}}^{z,w}$
- 6:   Compute condition prediction  $\hat{y} = g_{\beta^{(j-1)}}(\hat{x})$
- 7:   Update classifier parameters:

$$\beta^{(j)} \leftarrow \beta^{(j-1)} - \gamma_1 \nabla_{\beta} \mathcal{L}_{\alpha}(q_{z|x}, q_{w|x,y}, g_{y|z}) \Big|_{\phi=\phi^{(j-1)}, \psi=\psi^{(j-1)}, \rho=\rho^{(j-1)}, \eta=\eta^{(j-1)}}$$

- 8:   Update encoder and decoder parameters,  $\Omega^{(j)} = (\phi^{(j)}, \psi^{(j)}, \rho^{(j)}, \eta^{(j)})$ ,

$$\Omega^{(j)} \leftarrow \Omega^{(j-1)} - \gamma_2 \nabla_{\phi, \psi, \rho, \eta} \mathcal{L}_{\alpha}(q_{z|x}, q_{w|x,y}, g_{y|z}) \Big|_{\beta=\beta^{(j)}}$$

- 9: **end for**

**Return:**  $\phi^{(J)}, \psi^{(J)}, \rho^{(J)}, \eta^{(J)}, \beta^{(J)}$

---

## 4 Comparison to previous approaches

Here we review VAE-based methods for disentangled representation learning, which form the primary basis for comparison with our approach. Broader related literature is discussed in Appendix A.

VAEs [Kingma and Welling, 2014] are generative models that learn latent representations by maximizing the evidence lower bound (ELBO) on the data log-likelihood:

$$\mathbb{E}_{q_{z|x}}[\log p(x|z)] - \text{D}_{\text{KL}}(q_{z|x} \| p_z) \leq \log p(x),$$

where  $(x, z) \sim p$ , and  $z|x \sim q$  is a latent variable inferred from data. VAEs consist of an encoder  $q_{z|x}$  that maps inputs to latent distributions, and a decoder  $p_{x|z}$  that reconstructs inputs from latent representations. The learning process frames posterior inference as KL-regularized optimization over a variational family  $\mathcal{Q}$  aiming to approximate the posterior  $p_{z|x}$  under a typically simple prior  $p(z)$ . Several VAE extensions were proposed to encourage disentanglement. These are discussed below.

**Conditional VAEs** [Sohn et al., 2015] incorporate supervision to the standard VAE model by conditioning both the encoder and decoder on an observed label  $y$ , yielding the following objective:

$$\mathbb{E}_{q_{z|x,y}}[\log p(x|z, y)] - \text{D}_{\text{KL}}(q(z|x, y) \| p(z)) \leq \log p(x|y).$$

While this allows controlled generation and partial disentanglement between  $z$  and  $y$ , the latent variable  $z$  is still inferred from both  $x$  and  $y$  and thus can encode condition-specific information.

**Conditional Subspace VAEs (CSVAEs)** [Kllys et al., 2018], explicitly factorize the latent space into a shared component  $z$  a label-specific component  $w$  (see Supplementary Figure 1a). Similarly, their hierarchical extension Beker et al. [2024] introduces an intermediate latent variable between  $x$  and  $(z, w)$ . As in our approach, to encourage disentanglement, CSVAEs introduce an adversarial regularization term that penalizes mutual information between  $z$  and  $y$ , thereby discouraging predictability of  $y$  from  $z$ . They are learned by optimizing the following lower bound on  $\log p(x|y)$ :

$$\mathbb{E}_{q_{z,w|x,y}}[\log p(x|w, y)] - \mathbb{E}_{q_{z|x}}[\int g(y|z) \log g(y|z) dy] - \text{D}_{\text{KL}}(q_{w|x,y} \| q_{w|y}) - \text{D}_{\text{KL}}(q_{z|x} \| p_z).$$

**Domain Invariant VAEs (DIVA) and Characteristic-capturing VAEs (CCVAE)** DIVA [Ilse et al., 2020] and CCVAE [Joy et al., 2020], shown in Supplementary Figure 1b, introduce two latent variables,  $z$  and  $w$ , where  $w$  captures label-related features by jointly optimizing a classifier  $p(w|y)$  jointly alongside the remaining objective. For fully supervised cases, the DIVA model optimizes

$$\mathbb{E}_{q_{z,w|x}}[\log p(x|z, w)] + \mathbb{E}_{q_{w|x}}[\log q(y|w)] - \text{D}_{\text{KL}}(q_{z|x} \| p_z) - \text{D}_{\text{KL}}(q_{w|x} \| p_{w|y}) \leq \log p(x, y).$$

This objective corresponds to the assumptions  $x \perp y | z, w$  and  $z \perp w$ . Similarly, CCVAEs optimize the following lower bound on  $\log p(x|y)$ :

$$\mathbb{E}_{q_{z,w|x,y}} \left[ \frac{q(y/w)}{q(y/x)} \log \frac{p(x|z,w)}{q(y|w)} \right] - \text{D}_{\text{KL}}(q_{z|x} \| p_{z|y}) - \text{D}_{\text{KL}}(q_{w|x} \| p_{w|y}) + \log q(y|x).$$

**Comparison:** In contrast to our approach, which relies on minimal independence Assumptions (1 -2), CSVAEs, DIVA, and CCVAE incorporate stronger structural assumptions directly into their objectives. Additionally, DIVA and CCVAE lack explicit mechanisms to remove residual dependence between  $z$  and  $y$ , often leading to information leakage into the shared representation.

## 5 Experiments

We evaluate DISCoVeR with existing methods on both synthetic datasets and real datasets. When applicable, we assess reconstruction quality using negative log-likelihood (NLL), root mean squared error (RMSE), and the absolute deviation from the optimal Bayes classifier on the completed reconstruction, denoted as  $\Delta - \text{Bayes}$ . We measure disentanglement using a neural estimation Belghazi et al. [2018] of the the mutual information  $I(z; w)$ . For all experiments, model architectures, hyper-parameters and all other implementation details are provided in Appendix E.

### 5.1 Simulated data

We begin with controlled synthetic experiments to isolate and visualize disentanglement.

#### 5.1.1 Parametric model

**Data generating model:** Consider a model where the observed data  $x$  is generated as a function of two latent variables  $z$  and  $w$ , and  $y$  are binary labels. Assume that the marginal distributions of the latent variables are given by  $z \sim \mathcal{N}(0, 1)$  and  $w \sim \mathcal{N}(0, 1)$ , and that the data  $x$  is generated as the sum of the two latent variables:  $x = z + w$ . Since  $z$  and  $w$  are both drawn from  $\mathcal{N}(0, 1)$ , it follows that  $x \sim \mathcal{N}(0, 2)$ . Finally, assume that the binary label is determined by the sign of  $w$ :  $y = 1$  if  $w > 0$ , and  $y = 0$  otherwise.

**Optimal disentanglement:** Given that  $z$  and  $w$  are independent and  $x = z + w$ , we have that  $p(z | x) = \mathcal{N}(z; \frac{x}{2}, \frac{1}{2})$ . Hence, given  $x$ , the best estimate for  $z$  is  $\frac{x}{2}$ . Note that when ignoring the label  $y$ , the conditional distribution  $p(w | x)$  is  $p(w | x) = \mathcal{N}(w; \frac{x}{2}, \frac{1}{2})$ . However, the observation of  $y$  (which indicates whether  $w$  is positive or negative) truncates this distribution:

$$p(w | x, y = 1) = \frac{\mathcal{N}(w; \frac{x}{2}, \frac{1}{2})}{\Phi(\frac{x}{\sqrt{2}})}, \quad p(w | x, y = 0) = \frac{\mathcal{N}(w; \frac{x}{2}, \frac{1}{2})}{1 - \Phi(\frac{x}{\sqrt{2}})}. \quad (11)$$

**Results:** Table 1 shows that DISCoVeR (ours) best approximates the analytic posteriors, resulting in the lowest deviation from the optimal Bayes classifier and the best reconstruction.

Table 1: Parametric model results: DISCoVeR (ours) outperforms all competitors across all metrics.

	NLL ↓	$D_{\text{KL}}(q_{z x}    p_{z x})$ ↓	$D_{\text{KL}}(q_{w x}    p_{w x})$ ↓	$\Delta - \text{Bayes}$ ↓
CSVAE - N.A.	1.810 ± 0.016	6.65 ± 3.46	23.61 ± 0.36	24.83 ± 0.04
CSVAE	1.786 ± 0.022	2.85 ± 1.11	23.98 ± 4.36	24.33 ± 1.28
HCSVAE - N.A.	1.784 ± 0.010	4.01 ± 0.07	25.82 ± 0.38	24.99 ± 0.01
HCSVAE	1.770 ± 0.004	3.99 ± 0.09	26.25 ± 0.59	24.99 ± 0.01
DIVA	1.788 ± 0.008	3.21 ± 1.52	12.88 ± 3.31	3.51 ± 0.32
CCVAE	1.785 ± 0.006	1.77 ± 0.81	12.95 ± 3.35	3.57 ± 0.15
DISCoVeR (ours)	<b>1.769 ± 0.003</b>	<b>0.17 ± 0.01</b>	<b>10.10 ± 0.73</b>	<b>0.1 ± 0.28</b>

#### 5.1.2 Noisy Swiss roll

**Dataset:** We use a noisy variant of the labeled Swiss Roll dataset [Marsland, 2014, Klys et al., 2018], generating  $n = 20,000$  and assigning binary labels based on a lengthwise split, with labels flipped at rate  $\rho$ . The common geometry (its projection along the 2D plane) remains intact, the conditional structure along the third axis becomes noisy. Figure 2A illustrates the setup.

**Optimal disentanglement:** Since the Swiss Roll is sliced at the center and label noise is applied uniformly, marginalizing over labels yields a symmetric spiral centered along the roll—i.e., the marginal posterior  $p(z | x)$  is label-invariant. In contrast, the conditional component retains a noisy but informative signal, with a uniform noise level of  $\rho = 0.3$ . As a result, the Bayes optimal classifier trained on any realistic representation is upper-bounded at 70% accuracy.

**Results:** Figure 2 presents qualitative and quantitative results, showing that DISCoVeR both models the label noise accurately and effectively disentangles shared and condition-specific structure. Notably, DISCoVeR captures the marginal data distribution, successfully recovering the expected spiral pattern, as shown in Figure 2B (right). Additionally, the results in Table 2 show that DISCoVeR achieves the lowest deviation from the optimal Bayes classifier and minimal information leakage between latent variables, while preserving reconstruction quality.

Table 2: Noisy Swiss roll results: DISCoVeR yields lowest deviation from optimal-Bayes, while maintaining low latent leakage and high reconstruction accuracy.

	$I(z; w) \downarrow$	NLL $\downarrow$	$\Delta - \text{Bayes} \downarrow$
CSVAE - N.A.	0.011	$3.303 \pm 0.003$	$23.88 \pm 12.02$
CSVAE	<b>0.002</b>	<b><math>3.302 \pm 0.003</math></b>	$17.99 \pm 14.58$
HCSVAE - N.A.	0.062	<b><math>3.302 \pm 0.002</math></b>	$30.00 \pm 0.00$
HCSVAE	0.003	<b><math>3.302 \pm 0.002</math></b>	$30.00 \pm 0.00$
DIVA	0.423	<b><math>3.302 \pm 0.003</math></b>	$1.88 \pm 1.05$
CCVAE	0.254	<b><math>3.302 \pm 0.002</math></b>	$2.21 \pm 0.84$
DISCoVeR (Ours)	0.004	<b><math>3.302 \pm 0.002</math></b>	<b><math>1.14 \pm 0.21</math></b>

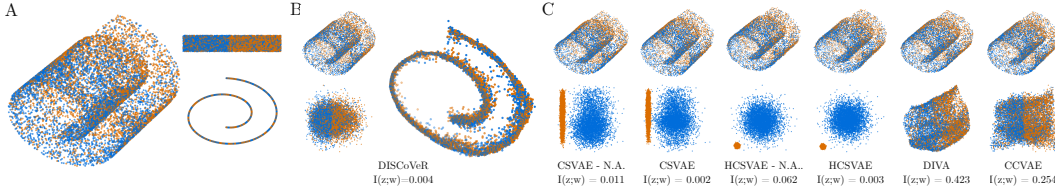


Figure 2: A: Noisy labeled Swiss Roll dataset. B (left): Reconstruction and conditional embedding from DISCoVeR. B (right): Marginal reconstruction from the shared embedding, recovering the spiral structure. C: Comparison of reconstruction and conditional embeddings across models.

## 5.2 Real data

### 5.2.1 Noisy colored MNIST

**Dataset:** We use a modified MNIST [Deng, 2012] dataset constructed from 60,000 duplicated images: in one copy we remove the red channel ( $y = 0$ ) and in the other we remove the green channel ( $y = 1$ ). The digit shape remains intact following the blue channel. Label noise is introduced by flipping labels with probability  $\rho \in \{0, 0.1, 0.2, 0.3, 0.4\}$ .

**Optimal disentanglement:** Since the colored images are generated in equal proportions, the marginal reconstruction for retains a single color (see Figure 3).

**Results:** We evaluate marginal coloring reconstruction by DISCoVeR and previous methods. Under no label noise ( $\rho = 0$ ), all methods perform similarly (Supplementary Figure 3). At all non-zero noise levels, DISCoVeR consistently outperforms competitors, whose marginal reconstructions are averaged over class-conditioned outputs. Metrics for  $\rho = 0.3$  are shown in Supplementary Table 2, with results for other noise levels in Supplementary Figure 4.

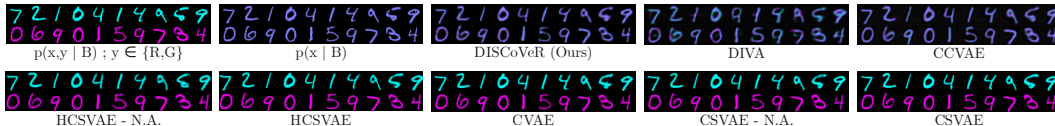


Figure 3: Colored MNIST results for noise level  $\rho = 0.3$ . DISCoVeR is the only model that consistently reconstructs the correct constant color matching the true marginal  $p(x|B)$ .

### 5.2.2 CelebA-Glasses

**Dataset:** We use all CelebA [Liu et al., 2015] images labeled with *eyeglasses* attribute ( $y = 1$ ), and twice as many randomly sampled images without ( $y = 0$ ), totaling  $n = 35,712$  samples.

**Results:** Figure 4 shows that DISCoVeR accurately reconstructs input images while producing shared embeddings that marginalize over the *eyeglasses* attribute, consistently adding "pseudoglasses" to all samples. Competing methods are shown in Supplementary Figure 5, with quantitative results in Supplementary Table 3. While reconstruction quality is comparable across methods, DISCoVeR achieves significantly better disentanglement.



Figure 4: CelebA-Eyeglasses results. Top: Original images with and without *eyeglasses*. Middle: Full reconstructions by DISCoVeR. Bottom: Reconstructions solely from common embeddings  $z$ .

### 5.2.3 Single cell RNA-sequencing (scRNA-seq) data from Lupus dataset

**Dataset:** We analyze single-cell RNA sequencing from  $n = 13,999$  peripheral blood mononuclear cells (PBMCs) collected from 8 lupus patients under two conditions: 7,451 cells control ( $y = 0$ ), and 6,548 IFN- $\beta$  stimulation cells. IFN- $\beta$  stimulation induces notable shifts in gene expression, visible in the UMAP embedding in Figure 5B (left).

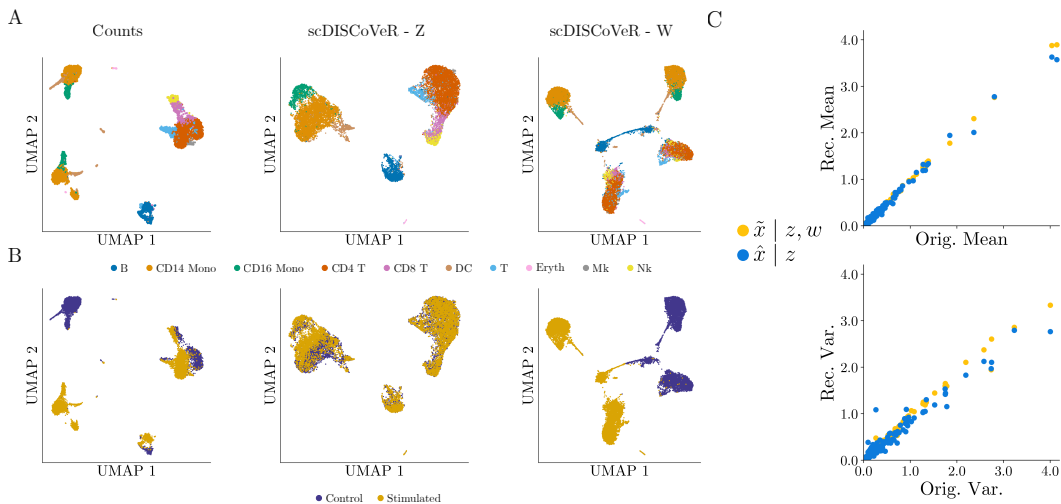


Figure 5: A, B (left): UMAP embeddings of gene counts from the IFN- $\beta$  stimulation dataset. A, B (middle): Common embedding  $z$  preserves cell type-specific differences, while correcting for the stimulation effect. A, B (right): Conditional embedding  $w$  captures the stimulation effect. C: Comparison of original and reconstructed log-mean (top) and log-variance (bottom) across cells for the two different reconstructions offered by DISCoVeR.

**Results:** Supplementary Table 5 shows that DISCoVeR effectively achieves the desired behavior with strong empirical performance, where only cell type information is captured in  $z$  (Figure 5A, middle) while the effects of IFN- $\beta$  stimulation are wholly represented in  $w$  (Figure 5B, right). Other approaches either (1) achieve mixing in the  $z$  space, but compromise on keeping cell types separated or (2) leak information about stimulation into the  $z$  space (Supplementary Figure 6).

**Facilitating interpretability:** By enabling marginalized reconstructions, DISCoVeR provides a direct link between shared embeddings and gene expression, offering clearer insight into the effects

of IFN- $\beta$  stimulation, unlike other methods. In Figure 5C, comparing variance across marginal and full reconstructions accurately recovers gene-level differences associated with IFN- $\beta$  stimulation, including *ISG15*, *FTL*, *CCL8*, *CXCL10*, *CXCL11*, *APOBEC3A*, *IL1RN*, *IFITM3* and *RSAD2*.

## 6 Conclusion

In this work we introduced a variational framework for disentangled representation learning that explicitly separates condition-invariant and condition-aware factors, while avoiding overly restrictive independence assumptions. Unlike prior work, DISCoVeR incorporates two reconstruction paths—one based solely on the shared latent variable  $z$ , and the other on the full pair  $(z, w)$ . Our model simultaneously learns informative shared representations, and captures structured variation across conditions. Experimental results demonstrate that DISCoVeR achieves strong reconstruction, minimal information leakage, and accurate modeling of conditional effects—consistently outperforming existing methods.

Our model assumes that the condition labels are fully observed and discrete. We leave extensions of our framework to semi-supervised or continuous condition settings for future work.

## References

- [1] Haleh Akrami, Anand A Joshi, Jian Li, Sergul Aydore, and Richard M Leahy. Brain lesion detection using a robust variational autoencoder and transfer learning. In *2020 IEEE 17th international symposium on biomedical imaging (ISBI)*, pages 786–790. IEEE, 2020.
- [2] Kei Akuzawa, Yusuke Iwasawa, and Yutaka Matsuo. Adversarial invariant feature learning with accuracy constraint for domain generalization. In *Machine Learning and Knowledge Discovery in Databases: European Conference, ECML PKDD 2019, Würzburg, Germany, September 16–20, 2019, Proceedings, Part II*, pages 315–331. Springer, 2020.
- [3] Martin Arjovsky, Léon Bottou, Ishaan Gulrajani, and David Lopez-Paz. Invariant risk minimization. *arXiv preprint arXiv:1907.02893*, 2019.
- [4] Ozgur Beker, Dreyton Amador, Jose Francisco Pomarino Nima, Simon Van Deursen, Yvon Woappi, and Bianca Dumitrascu. Patches: A representation learning framework for decoding shared and condition-specific transcriptional programs in wound healing. *bioRxiv*, pages 2024–12, 2024.
- [5] Mohamed Ishmael Belghazi, Aristide Baratin, Sai Rajeshwar, Sherjil Ozair, Yoshua Bengio, Aaron Courville, and Devon Hjelm. Mutual information neural estimation. In Jennifer Dy and Andreas Krause, editors, *Proceedings of the 35th International Conference on Machine Learning*, volume 80 of *Proceedings of Machine Learning Research*, pages 531–540. PMLR, 10–15 Jul 2018. URL <https://proceedings.mlr.press/v80/belghazi18a.html>.
- [6] Aharon Ben-Tal, Dick Den Hertog, Anja De Waegenare, Bertrand Melenberg, and Gijs Rennen. Robust solutions of optimization problems affected by uncertain probabilities. *Management Science*, 59(2):341–357, 2013.
- [7] Pierre Boyeau, Justin Hong, Adam Gayoso, Martin Kim, José L McFaline-Figueroa, Michael I Jordan, Elham Azizi, Can Ergen, and Nir Yosef. Deep generative modeling of sample-level heterogeneity in single-cell genomics. *BioRxiv*, pages 2022–10, 2022.
- [8] Fabio Maria Carlucci, Paolo Russo, Tatiana Tommasi, and Barbara Caputo. Hallucinating agnostic images to generalize across domains. In *2019 IEEE/CVF International Conference on Computer Vision Workshop (ICCVW)*, pages 3227–3234. IEEE, 2019.
- [9] Jianting Chen, Ling Ding, Yunxiao Yang, Zaiyuan Di, and Yang Xiang. Domain adversarial active learning for domain generalization classification. *IEEE Transactions on Knowledge and Data Engineering*, 2024.
- [10] Sheng Cheng, Tejas Gokhale, and Yezhou Yang. Adversarial bayesian augmentation for single-source domain generalization. In *Proceedings of the IEEE/CVF International Conference on Computer Vision*, pages 11400–11410, 2023.
- [11] Aveen Dayal, Vimal KB, Linga Reddy Cenkeramaddi, C Mohan, Abhinav Kumar, and Vineeth N Balasubramanian. Madg: margin-based adversarial learning for domain generalization. *Advances in Neural Information Processing Systems*, 36:58938–58952, 2023.
- [12] Li Deng. The mnist database of handwritten digit images for machine learning research. *IEEE Signal Processing Magazine*, 29(6):141–142, 2012.
- [13] Zhengming Ding and Yun Fu. Deep domain generalization with structured low-rank constraint. *IEEE Transactions on Image Processing*, 27(1):304–313, 2017.
- [14] John C Duchi and Hongseok Namkoong. Learning models with uniform performance via distributionally robust optimization. *The Annals of Statistics*, 49(3):1378–1406, 2021.
- [15] John C Duchi, Peter W Glynn, and Hongseok Namkoong. Statistics of robust optimization: A generalized empirical likelihood approach. *Mathematics of Operations Research*, 46(3): 946–969, 2021.
- [16] Bradley Efron. Two modeling strategies for empirical bayes estimation. *Statistical science: a review journal of the Institute of Mathematical Statistics*, 29(2):285, 2014.

- [17] Li Fei-Fei, Rob Fergus, and Pietro Perona. One-shot learning of object categories. *IEEE transactions on pattern analysis and machine intelligence*, 28(4):594–611, 2006.
- [18] Kuzman Ganchev, Joao Graça, Jennifer Gillenwater, and Ben Taskar. Posterior regularization for structured latent variable models. *The Journal of Machine Learning Research*, 11:2001–2049, 2010.
- [19] Muhammad Ghifary, W Bastiaan Kleijn, Mengjie Zhang, and David Balduzzi. Domain generalization for object recognition with multi-task autoencoders. In *Proceedings of the IEEE international conference on computer vision*, pages 2551–2559, 2015.
- [20] William J Godinez, Eric J Ma, Alexander T Chao, Luying Pei, Peter Skewes-Cox, Stephen M Canham, Jeremy L Jenkins, Joseph M Young, Eric J Martin, and W Armand Guiguemde. Design of potent antimalarials with generative chemistry. *Nature Machine Intelligence*, 4(2):180–186, 2022.
- [21] Tejas Gokhale, Rushil Anirudh, Jayaraman J Thiagarajan, Bhavya Kailkhura, Chitta Baral, and Yezhou Yang. Improving diversity with adversarially learned transformations for domain generalization. In *Proceedings of the IEEE/CVF Winter Conference on Applications of Computer Vision*, pages 434–443, 2023.
- [22] Ian Goodfellow, Jean Pouget-Abadie, Mehdi Mirza, Bing Xu, David Warde-Farley, Sherjil Ozair, Aaron Courville, and Yoshua Bengio. Generative adversarial networks. *Communications of the ACM*, 63(11):139–144, 2020.
- [23] Raia Hadsell, Sumit Chopra, and Yann LeCun. Dimensionality reduction by learning an invariant mapping. In *2006 IEEE Computer Society Conference on Computer Vision and Pattern Recognition (CVPR'06)*, volume 2, pages 1735–1742. IEEE, 2006.
- [24] Irina Higgins, Loic Matthey, Arka Pal, Christopher Burgess, Xavier Glorot, Matthew Botvinick, Shakir Mohamed, and Alexander Lerchner. beta-vae: Learning basic visual concepts with a constrained variational framework. In *International conference on learning representations*, 2017.
- [25] Jonathan Ho, Ajay Jain, and Pieter Abbeel. Denoising diffusion probabilistic models. *Advances in neural information processing systems*, 33:6840–6851, 2020.
- [26] Elad Hoffer and Nir Ailon. Deep metric learning using triplet network. In *International workshop on similarity-based pattern recognition*, pages 84–92. Springer, 2015.
- [27] Badr Youbi Idrissi, Martin Arjovsky, Mohammad Pezeshki, and David Lopez-Paz. Simple data balancing achieves competitive worst-group-accuracy. In *Conference on Causal Learning and Reasoning*, pages 336–351. PMLR, 2022.
- [28] Maximilian Ilse, Jakub M Tomczak, Christos Louizos, and Max Welling. Diva: Domain invariant variational autoencoders. In *Medical Imaging with Deep Learning*, pages 322–348. PMLR, 2020.
- [29] Tom Joy, Sebastian M Schmon, Philip HS Torr, N Siddharth, and Tom Rainforth. Capturing label characteristics in vaes. *arXiv preprint arXiv:2006.10102*, 2020.
- [30] Daehee Kim, Youngjun Yoo, Seunghyun Park, Jinkyu Kim, and Jaekoo Lee. Selfreg: Self-supervised contrastive regularization for domain generalization. In *Proceedings of the IEEE/CVF international conference on computer vision*, pages 9619–9628, 2021.
- [31] Diederik P Kingma and Max Welling. Auto-encoding variational bayes. *International Conference on Learning Representations*, 2014.
- [32] Jack Klys, Jake Snell, and Richard Zemel. Learning latent subspaces in variational autoencoders. *Advances in neural information processing systems*, 31, 2018.
- [33] Gregory Koch, Richard Zemel, Ruslan Salakhutdinov, et al. Siamese neural networks for one-shot image recognition. In *International Conference on Machine Learning (ICML) deep learning workshop*, volume 2, 2015.

- [34] David Krueger, Ethan Caballero, Joern-Henrik Jacobsen, Amy Zhang, Jonathan Binas, Dinghui Zhang, Remi Le Priol, and Aaron Courville. Out-of-distribution generalization via risk extrapolation (rex). In *International Conference on Machine Learning*, pages 5815–5826. PMLR, 2021.
- [35] Hugo Larochelle, Dumitru Erhan, and Yoshua Bengio. Zero-data learning of new tasks. In *AAAI*, volume 1, page 3, 2008.
- [36] Anders Boesen Lindbo Larsen, Søren Kaae Sønderby, Hugo Larochelle, and Ole Winther. Autoencoding beyond pixels using a learned similarity metric. In Maria Florina Balcan and Kilian Q. Weinberger, editors, *Proceedings of The 33rd International Conference on Machine Learning*, volume 48 of *Proceedings of Machine Learning Research*, pages 1558–1566, New York, New York, USA, 20–22 Jun 2016. PMLR. URL <https://proceedings.mlr.press/v48/larsen16.html>.
- [37] Ya Li, Mingming Gong, Xinmei Tian, Tongliang Liu, and Dacheng Tao. Domain generalization via conditional invariant representations. In *Proceedings of the AAAI conference on artificial intelligence*, volume 32, 2018.
- [38] Yunsheng Li and Nuno Vasconcelos. Efficient multi-domain learning by covariance normalization. In *Proceedings of the IEEE/CVF Conference on Computer Vision and Pattern Recognition*, pages 5424–5433, 2019.
- [39] Evan Z Liu, Behzad Haghgoo, Annie S Chen, Aditi Raghunathan, Pang Wei Koh, Shiori Sagawa, Percy Liang, and Chelsea Finn. Just train twice: Improving group robustness without training group information. In *International Conference on Machine Learning*, pages 6781–6792. PMLR, 2021.
- [40] Ziwei Liu, Ping Luo, Xiaogang Wang, and Xiaoou Tang. Deep learning face attributes in the wild. In *Proceedings of International Conference on Computer Vision (ICCV)*, December 2015.
- [41] Romain Lopez, Jeffrey Regier, Michael B Cole, Michael I Jordan, and Nir Yosef. Deep generative modeling for single-cell transcriptomics. *Nature methods*, 15(12):1053–1058, 2018.
- [42] Ilya Loshchilov and Frank Hutter. Decoupled weight decay regularization. In *International Conference on Learning Representations*, 2019. URL <https://openreview.net/forum?id=Bkg6RiCqY7>.
- [43] Mohammad Lotfollahi, F Alexander Wolf, and Fabian J Theis. scgen predicts single-cell perturbation responses. *Nature methods*, 16(8):715–721, 2019.
- [44] Mario Lovrić, Tomislav Đuričić, Han TN Tran, Hussain Hussain, Emanuel Lacić, Morten A Rasmussen, and Roman Kern. Should we embed in chemistry? a comparison of unsupervised transfer learning with pca, umap, and vae on molecular fingerprints. *Pharmaceuticals*, 14(8):758, 2021.
- [45] Massimiliano Mancini, Samuel Rota Buló, Barbara Caputo, and Elisa Ricci. Best sources forward: domain generalization through source-specific nets. In *2018 25th IEEE international conference on image processing (ICIP)*, pages 1353–1357. IEEE, 2018.
- [46] Stephen Marsland. *Machine Learning: An Algorithmic Perspective, Second Edition*. Chapman & Hall/CRC, 2nd edition, 2014. ISBN 1466583282.
- [47] Saeid Motiian, Marco Piccirilli, Donald A Adjeroh, and Gianfranco Doretto. Unified deep supervised domain adaptation and generalization. In *Proceedings of the IEEE international conference on computer vision*, pages 5715–5725, 2017.
- [48] Krikamol Muandet, David Balduzzi, and Bernhard Schölkopf. Domain generalization via invariant feature representation. In *International conference on machine learning*, pages 10–18. PMLR, 2013.
- [49] Usman Muhammad, Jorma Laaksonen, Djamila Romaissa Beddiar, and Mourad Oussalah. Domain generalization via ensemble stacking for face presentation attack detection. *International Journal of Computer Vision*, 132(12):5759–5782, 2024.

- [50] Hyun Oh Song, Yu Xiang, Stefanie Jegelka, and Silvio Savarese. Deep metric learning via lifted structured feature embedding. In *Proceedings of the IEEE conference on computer vision and pattern recognition*, pages 4004–4012, 2016.
- [51] Kazuki Omi, Jun Kimata, and Toru Tamaki. Model-agnostic multi-domain learning with domain-specific adapters for action recognition. *IEICE TRANSACTIONS on Information and Systems*, 105(12):2119–2126, 2022.
- [52] Sinno Jialin Pan, Qiang Yang, et al. A survey on transfer learning. *IEEE Transactions on knowledge and data engineering*, 22(10):1345–1359, 2010.
- [53] F. Pedregosa, G. Varoquaux, A. Gramfort, V. Michel, B. Thirion, O. Grisel, M. Blondel, P. Prettenhofer, R. Weiss, V. Dubourg, J. Vanderplas, A. Passos, D. Cournapeau, M. Brucher, M. Perrot, and E. Duchesnay. Scikit-learn: Machine learning in Python. *Journal of Machine Learning Research*, 12:2825–2830, 2011.
- [54] Jonas Peters, Peter Bühlmann, and Nicolai Meinshausen. Causal inference by using invariant prediction: identification and confidence intervals. *Journal of the Royal Statistical Society Series B: Statistical Methodology*, 78(5):947–1012, 2016.
- [55] Jonas Peters, Dominik Janzing, and Bernhard Schölkopf. *Elements of causal inference: foundations and learning algorithms*. The MIT Press, 2017.
- [56] Vihari Piratla, Praneeth Netrapalli, and Sunita Sarawagi. Focus on the common good: Group distributional robustness follows. In *International Conference on Learning Representations*, 2021.
- [57] Sylvestre-Alvise Rebuffi, Hakan Bilen, and Andrea Vedaldi. Learning multiple visual domains with residual adapters. *Advances in neural information processing systems*, 30, 2017.
- [58] Sylvestre-Alvise Rebuffi, Hakan Bilen, and Andrea Vedaldi. Efficient parametrization of multi-domain deep neural networks. In *Proceedings of the IEEE conference on computer vision and pattern recognition*, pages 8119–8127, 2018.
- [59] H Robbins. An empirical bayes approach to statistics. *Proceedings of the Third Berkeley Symposium on Mathematical Statistics and Probability, 1954–1955, vol. 1*, 1956.
- [60] Shiori Sagawa, Pang Wei Koh, Tatsunori B Hashimoto, and Percy Liang. Distributionally robust neural networks. In *International Conference on Learning Representations*, 2019.
- [61] Yuli Slavutsky and Yuval Benjamini. Class distribution shifts in zero-shot learning: Learning robust representations. *Advances in Neural Information Processing Systems*, 37:89213–89248, 2024.
- [62] Jascha Sohl-Dickstein, Eric Weiss, Niru Maheswaranathan, and Surya Ganguli. Deep unsupervised learning using nonequilibrium thermodynamics. In *International conference on machine learning*, pages 2256–2265. pmlr, 2015.
- [63] Kihyuk Sohn. Improved deep metric learning with multi-class n-pair loss objective. *Advances in neural information processing systems*, 29, 2016.
- [64] Kihyuk Sohn, Honglak Lee, and Xinchen Yan. Learning structured output representation using deep conditional generative models. *Advances in neural information processing systems*, 28, 2015.
- [65] Baochen Sun and Kate Saenko. Deep coral: Correlation alignment for deep domain adaptation. In *Computer vision—ECCV 2016 workshops: Amsterdam, the Netherlands, October 8–10 and 15–16, 2016, proceedings, part III 14*, pages 443–450. Springer, 2016.
- [66] Yoav Wald, Amir Feder, Daniel Greenfeld, and Uri Shalit. On calibration and out-of-domain generalization. *Advances in neural information processing systems*, 34:2215–2227, 2021.
- [67] Haohan Wang, Aaksha Meghawat, Louis-Philippe Morency, and Eric P Xing. Select-additive learning: Improving generalization in multimodal sentiment analysis. In *2017 IEEE International Conference on Multimedia and Expo (ICME)*, pages 949–954. IEEE, 2017.

- [68] Haohan Wang, Eric P Xing, Zexue He, and Zachary C Lipton. Learning robust representations by projecting superficial statistics out. In *7th International Conference on Learning Representations, ICLR 2019*, 2019.
- [69] Jiaheng Wei, Harikrishna Narasimhan, Ehsan Amid, Wen-Sheng Chu, Yang Liu, and Abhishek Kumar. Distributionally robust post-hoc classifiers under prior shifts. In *International Conference on Learning Representations (ICLR)*, 2023.
- [70] Chao-Yuan Wu, R Manmatha, Alexander J Smola, and Philipp Krahenbuhl. Sampling matters in deep embedding learning. In *Proceedings of the IEEE international conference on computer vision*, pages 2840–2848, 2017.
- [71] Chenling Xu, Romain Lopez, Edouard Mehlman, Jeffrey Regier, Michael I Jordan, and Nir Yosef. Probabilistic harmonization and annotation of single-cell transcriptomics data with deep generative models. *Molecular systems biology*, 17(1):e9620, 2021.
- [72] Tongtong Yuan, Weihong Deng, Jian Tang, Yinan Tang, and Binghui Chen. Signal-to-noise ratio: A robust distance metric for deep metric learning. In *Proceedings of the IEEE/CVF conference on computer vision and pattern recognition*, pages 4815–4824, 2019.
- [73] Jiuzi Zhang, Xiang Li, Jilun Tian, Yuchen Jiang, Hao Luo, and Shen Yin. A variational local weighted deep sub-domain adaptation network for remaining useful life prediction facing cross-domain condition. *Reliability Engineering & System Safety*, 231:108986, 2023.
- [74] Kaiyang Zhou, Yongxin Yang, Yu Qiao, and Tao Xiang. Domain adaptive ensemble learning. *IEEE Transactions on Image Processing*, 30:8008–8018, 2021.
- [75] Wei Zhu, Le Lu, Jing Xiao, Mei Han, Jiebo Luo, and Adam P Harrison. Localized adversarial domain generalization. In *Proceedings of the IEEE/CVF conference on computer vision and pattern recognition*, pages 7108–7118, 2022.

## A Additional related work

### A.1 Domain Generalization

The task of representation disentanglement is closely related to the field of domain generalization [48], which assumes limited or no access to target domain samples and aims to learn representations that can be readily adapted, often via transfer learning, to new, unseen domains.

As noted by Wang et al. [68], existing methods in domain generalization can be broadly categorized into two main approaches: (i) approaches for reducing the inter-domain differences, often by using adversarial techniques [19, 67, 47, 37, 8, 37, 68, 2, 75, 21, 11, 10, 9], and (ii) Approaches that construct an ensemble of domain-specific models, and then fuse their representations to form a unified, domain-agnostic representation [13, 45, 74, 49].

Additional strategies for domain generalization include contrastive learning approaches [30], methods based on distribution alignment via metrics [48, 65], and techniques utilizing custom network architectures, for instance by incorporating domain-specific adapters between shared layers [57, 58, 38, 51].

The primary distinction between these methods and ours lies in the explicit probabilistic modeling and disentanglement of domain-invariant and domain-specific factors. Whereas prior approaches typically focus on aligning domains through adversarial training or fusing multiple domain-specific predictors, our method constructs a structured latent space, decomposed into a shared representation  $z$ , capturing domain-invariant information, and a conditional component  $w$ , which encodes domain-specific variability. This factorization is learned through a tailored variational objective involving an adversarial penalty and two reconstructions—one based on  $z$  alone, and another on the full latent pair  $(z, w)$ , thereby promoting both interpretability and a clean separation of shared and domain-aware features.

### A.2 Out of distribution generalization

#### A.2.1 Environment balancing methods

The field of out-of-distribution (OOD) generalization emerged from foundational work on causality and invariance across training environments [54, 55]. The central assumption is that each environment exhibits distinct spurious correlations between features and labels; therefore, robust generalization requires models to focus on invariant relationships that hold across environments. To address this distribution shift, many recent approaches adopt a regularized empirical risk minimization framework:

$$\min_{\theta} \sum_{e \in E_{\text{train}}} \ell^e(f_{\theta}) + \lambda R(f_{\theta}, E_{\text{train}}), \quad (12)$$

where the regularizer  $R$  encourages representations that are stable across environments. Among these, Invariant Risk Minimization (IRM) [3] enforces that a single classifier remains optimal across all environments, Variance Risk Extrapolation (VarREx) [34] promotes robustness by minimizing the variance of losses across environments, and CLOvE [66] takes a calibration-theoretic perspective, penalizing discrepancies between predicted confidence and correctness across environments.

While these methods focus on enforcing predictive invariance across environments through regularization, our approach instead explicitly enforces conditional independence between the shared latent variable  $z$  and an environment-aware variable  $w$ .

#### A.2.2 Distributionally robust methods

An alternative line of work for handling distribution shifts is Distributionally Robust Optimization (DRO) [6, 15, 14, 69], which avoids assuming a fixed data-generating distribution. Instead, DRO methods optimize performance under the worst-case scenario over a family of plausible distributions. A prominent variant, known as group DRO [60, 56], introduces group-level structure that may correlate with spurious features, potentially leading to biased predictions. In settings where group labels are not directly observed, several strategies have been proposed, including reweighting high-loss examples [39] and balancing class-group combinations through data sub-sampling [27].

However, these approaches assume that the label space remains fixed between training and test time, limiting their applicability in adaptation to new domains, environments or conditions.

### A.3 Zero-shot learning

Zero-shot learning systems [17, 35] aim to classify instances from novel, previously unseen classes at test time. In contrast to the out-of-distribution (OOD) generalization setting, these approaches typically do not assume the presence or structure of a distribution shift. Instead, a common strategy is to learn data representations that capture class-agnostic similarity, enabling the model to determine whether two instances belong to the same class without requiring knowledge of the class identity itself. Such methods include contrastive-learning [23], siamese neural networks [33], triplet networks [26], and other more recent variations [50, 63, 70, 72]. Recent work has begun to address the impact of class distribution shifts in zero-shot settings. For instance, Slavutsky and Benjamini [61] integrate environment-based regularization—motivated by OOD generalization—with zero-shot learning by simulating distribution shifts through hierarchical sampling, enabling the model to learn representations that are robust to shifts in class distributions.

While this line of work shares our motivation of improving robustness under unseen conditions, it primarily addresses the problem of class-level generalization through similarity-based learning, rather than explicitly modeling and disentangling the latent factors—such as domain or environment—that drive distributional variation across tasks.

## B Proofs

### B.1 Proof of Proposition 2.1

*Proof.*

$$\text{ELBO}(q, p; x, y) - \mathcal{L}_w(q_{w|x,y}, p; x, y) \quad (13)$$

$$= [\log p(x | y) - \text{D}_{\text{KL}}(q_{w|x,y} \| p_{w|x,y})] - [\log p(x | y) - \text{D}_{\text{KL}}(q_{z|x}q_{w|x,y} \| p_{z,w|x,y})] \quad (14)$$

$$= \text{D}_{\text{KL}}(q_{z|x}q_{w|x,y} \| p_{z,w|x,y}) - \text{D}_{\text{KL}}(q_{w|x,y} \| p_{w|x,y}) \quad (15)$$

$$= \mathbb{E}_{q_{w|x,y}} [\mathbb{E}_{q_{z|x}} [\log q(z | x) + \log q(w|x, y) - \log p(z, w | x, y)]] \quad (16)$$

$$- \mathbb{E}_{q_{w|x,y}} [\log q(w|x, y) - \log p(w|x, y)] \quad (17)$$

$$= \mathbb{E}_{q_{w|x,y}} [\mathbb{E}_{q_{z|x}} [\log q(z | x) - \log p(z, w | x, y) + \log p(w|x, y)]] \quad (18)$$

$$= \mathbb{E}_{q_{z|x}} [\log q(z | x) - \log p(z | w, x, y)] \quad (19)$$

$$= \text{D}_{\text{KL}}(q_{z|x} \| p_{z|w,x,y}). \quad (20)$$

□

### B.2 Game equilibrium

#### B.2.1 Regularity conditions

To ensure that expectations and KL-terms in the game objective  $\mathcal{L}(q_{z|x}, q_{w|x,y}, g_{y|z})$  render the functionals strictly concave in  $q_{z|x}$ , strictly concave in  $q_{w|x,y}$ , and strictly convex in  $g$ , the following regularity conditions are required:

1. The likelihoods  $p(x|z), p(x|z, w), p(y|x)$  are strictly positive, continuous densities.
2. The variational families  $Q_z$  and  $Q_w$ , and the set of achievable classifiers  $\mathcal{G}$  are non-empty, convex and compact.
3.  $\log p(x|z, w)$  and  $\log g(y|x)$  are integrable.

#### B.2.2 Proof of Proposition 2.2

*Proof.* Since  $\mathcal{L}_z(q_{z|x}, p; x)$  is the standard ELBO objective, we have that

$$\mathcal{L}_z(q_{z|x}, p; x) = \log p(x) - \text{D}_{\text{KL}}(q_{z|x} \| p_{z|x}). \quad (21)$$

Similarly, we have that

$$\mathcal{L}_w(q_{w|x,y}, p; x, y) = \log p(x | y) - \text{D}_{\text{KL}}(q_{z|x}q_{w|x,y} \| p_{z,w|x,y}). \quad (22)$$

Thus,

$$\mathcal{L}(q_{z|x}, q_{w|x,y}, g_{y|z}) = \mathbb{E}_{p_{x,y}} [\log p(x) - \text{D}_{\text{KL}}(q_{z|x} \| p_{z|x})] \quad (23)$$

$$+ \log p(x | y) - \text{D}_{\text{KL}}(q_{z|x} q_{w|x,y} \| p_{z,w|x,y}) \quad (24)$$

$$- \mathbb{E}_{q_{z|x}} \log g(y | z)]. \quad (25)$$

For fixed  $q_{z|x}$ , the adversarial classifier minimizes:

$$- \mathbb{E}_{p_{x,y}} \mathbb{E}_{q_{z|x}} \log g(y | z), \quad (26)$$

which is the population cross-entropy and is strictly convex in  $g(y|z)$ , and thus has a unique solution.

It remains to show that the terms in the objective function that depend on  $q_{z|x}$  and  $q_{w|x,y}$ , are strictly concave in each argument when the others are held fixed.

Focusing on the terms dependent on  $q_{w|x,y}$  first, define

$$\ell_w := - \text{D}_{\text{KL}}(q_{z|x} q_{w|x,y} \| p_{z,w|x,y}) \quad (27)$$

$$= - \iint q(z|x) q(w|x,y) [\log q(z|x) + \log q(w|x,y) - \log p(z,w|x,y)] dz dw$$

$$= - \int q(z|x) \log q(z|x) dz + \int q(w|x,y) \log q(w|x,y) dw \quad (28)$$

$$- \iint q(z|x) q(w|x,y) \log p(z,w|x,y) dz dw \quad (29)$$

$$= H(q_{z|x}) + H(q_{w|x,y}) + \mathbb{E}_{q_{z|x}} \mathbb{E}_{q_{w|x,y}} \log p(z,w|x,y). \quad (30)$$

Note that

$$\mathbb{E}_{q_{z|x}} \mathbb{E}_{q_{w|x,y}} \log p(z,w|x,y) \quad (31)$$

is linear in  $q_{w|x,y}$ , and since  $H(q_{w|x,y})$  is strictly concave in  $q_{w|x,y}$ , we have that  $\mathbb{E}_{p_{x,y}}[\ell_w]$  is strictly concave in  $q_{w|x,y}$ .

Similarly, define

$$\ell_z := - \text{D}_{\text{KL}}(q_{z|x} \| p_{z|x}) - \text{D}_{\text{KL}}(q_{z|x} q_{w|x,y} \| p_{z,w|x,y}). \quad (32)$$

By convexity of KL divergence in its first argument,  $- \text{D}_{\text{KL}}(q_{z|x} \| p_{z|x})$  is strictly concave in  $q_{z|x}$ .

Focusing on the second KL term, from Equation 30 we have that

$$- \text{D}_{\text{KL}}(q_{z|x} q_{w|x,y} \| p_{z,w|x,y}) = H(q_{z|x}) + H(q_{w|x,y}) + \mathbb{E}_{q_{z|x}} \mathbb{E}_{q_{w|x,y}} \log p(z,w|x,y), \quad (33)$$

where  $H(q_{z|x})$  is strictly concave in  $q_{z|x}$ .

Recall that we assumed that  $p(w|y)$  depends on  $q(z|x)$ . Under our model

$$p(x,y,z,w) = p(y)p(w|y)p(z)p(x|z,w), \quad (34)$$

yielding

$$p(z,w|x,y) = p(w|y) \frac{p(z)p(x|z,w)}{p(x|y)}. \quad (35)$$

Hence,

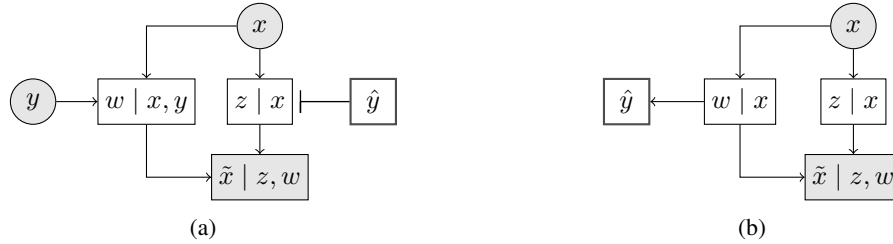
$$\mathbb{E}_{q_{z|x}} \mathbb{E}_{q_{w|x,y}} \log p(z,w|x,y) = \mathbb{E}_{q_{z|x}} \mathbb{E}_{q_{w|x,y}} \left[ \log p(w|y) + \log \frac{p(z)p(x|z,w)}{p(x|y)} \right],$$

where  $p(w|y) = \mathcal{N}(w; \mu_y, I)$  with  $\mu_y = \mathbb{E}_{p_{x|y}}[\mathbb{E}_{q_{z|x}}[z]]$ . Therefore,

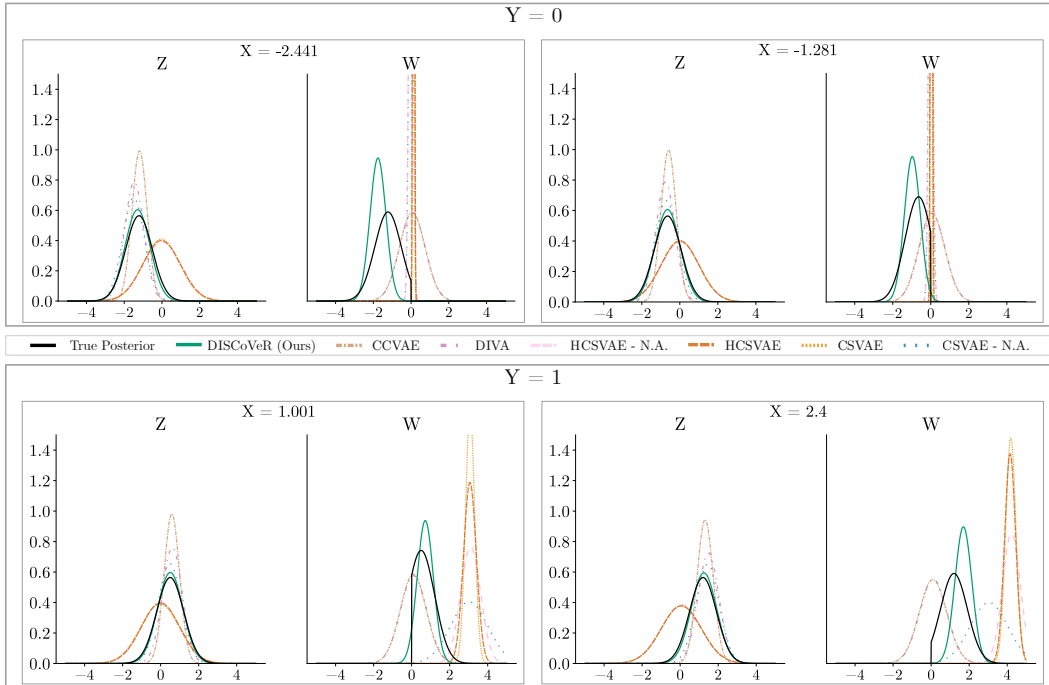
$$\mathbb{E}_{q_{z|x}} \mathbb{E}_{q_{w|x,y}} [\log p(w|y)] = -\frac{1}{2} \left[ d \log(2\pi) + \mathbb{E}_{q_{z|x}} \mathbb{E}_{q_{w|x,y}} \|w - \mu_y\|^2 \right] \quad (36)$$

where  $-\|w - \mu_y\|^2$  is a quadratic form in  $\mu_y$ , which is linear in  $q_{z|x}$ , and thus  $\mathbb{E}_{q_{z|x}} \mathbb{E}_{q_{w|x,y}} [\log p(w|y)]$  is strictly concave in  $q_{z|x}$ . Hence,  $- \text{D}_{\text{KL}}(q_{z|x} q_{w|x,y} \| p_{z,w|x,y})$  is strictly concave in  $q_{z|x}$ , and thus so is  $\mathbb{E}_{p_{x,y}}[\ell_z]$ .  $\square$

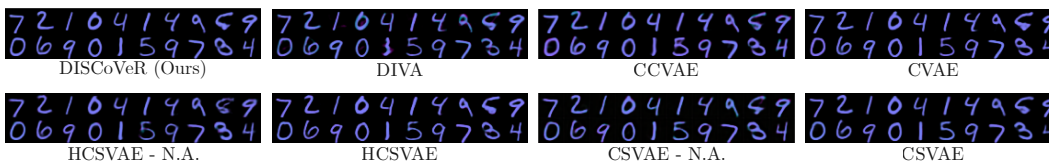
## C Supplementary Figures



Supplementary Figure 1: Encoder-decoder structures for previous approaches. (a) CSVAE. (b) DIVA-CCVAE.



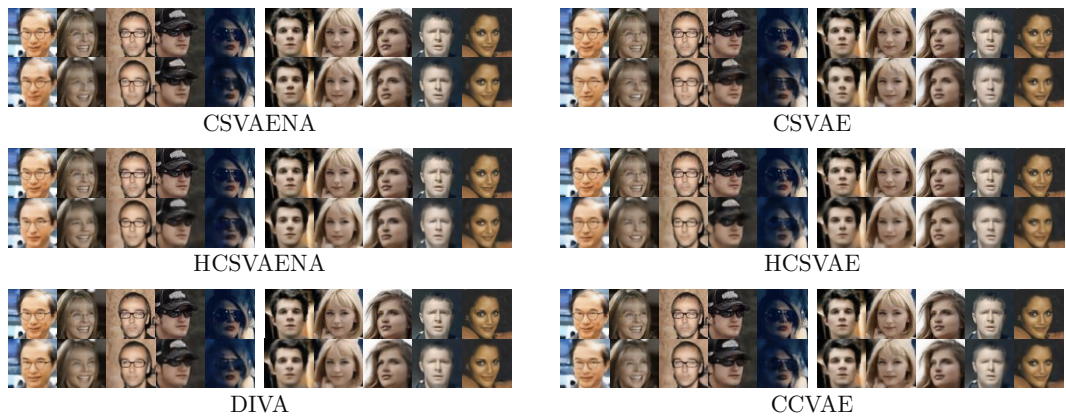
Supplementary Figure 2: Comparison of approximate variational posteriors against the true posterior for latent variables  $z, w$  for different values of  $x$  with  $y = 0$  (top) and  $y = 1$  (bottom).



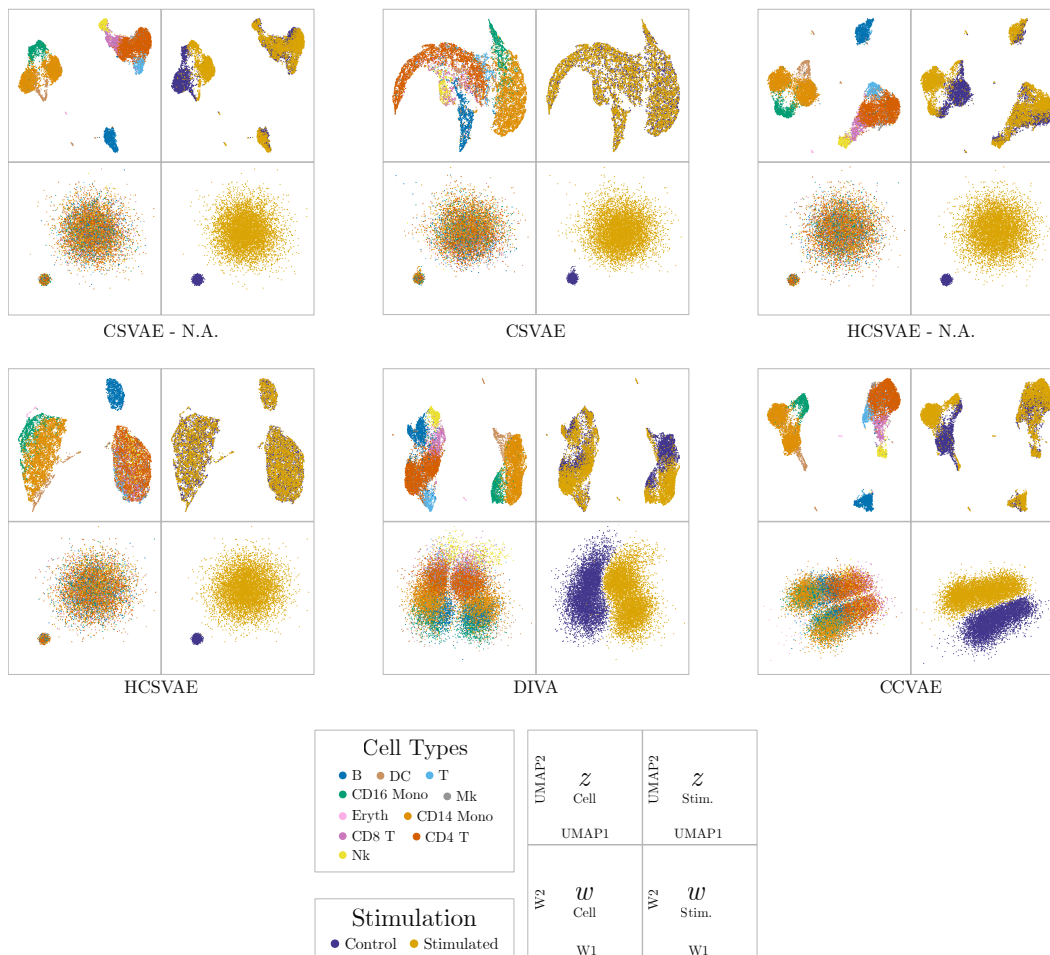
Supplementary Figure 3: Colored MNIST results for no noise.



Supplementary Figure 4: Colored MNIST visual results across the remaining noise levels.



Supplementary Figure 5: Reconstruction performance for other models on the CelebA-Glasses dataset. Top: Original samples from the data. Bottom: Reconstructions by the given model.



Supplementary Figure 6: Embeddings obtained by other models on the Kang dataset. For each block, top (resp. bottom) rows are  $z$  (resp.  $w$ ) embeddings, while left (resp. right) columns are colored by cell type (resp. stimulation).

## D Supplementary Tables

Supplementary Table 1: RMSE for the Colored MNIST dataset without any label noise.

	Marginal RMSE ( $\rho = 0$ ) ↓
CSVAE - No Adv.	<b>0.064 ± 0.002</b>
CSVAE	0.079 ± 0.008
HCSVAE - No Adv.	0.094 ± 0.004
HCSVAE	0.079 ± 0.030
DIVA	0.065 ± 0.005
CCVAE	0.065 ± 0.006
<b>DISCoVeR (Ours)</b>	<b>0.064 ± 0.000</b>

Supplementary Table 2: RMSE calculated between the estimated and true marginal across different levels of label noise on the Colored MNIST dataset.  $p$  defines label flip probability. Bold denotes best performance.

	Marginal RMSE ↓			
	$p = 0.1$	$p = 0.2$	$p = 0.3$	$p = 0.4$
CSVAE - No Adv.	0.141 ± 0.002	0.141 ± 0.003	0.142 ± 0.002	0.143 ± 0.002
CSVAE	0.135 ± 0.022	0.152 ± 0.018	0.181 ± 0.007	0.173 ± 0.008
HCSVAE - No Adv.	0.150 ± 0.001	0.150 ± 0.000	0.151 ± 0.000	0.151 ± 0.001
HCSVAE	0.139 ± 0.003	0.141 ± 0.001	0.141 ± 0.001	0.141 ± 0.001
DIVA	0.115 ± 0.011	0.102 ± 0.013	0.106 ± 0.010	0.113 ± 0.014
CCVAE	0.092 ± 0.002	0.103 ± 0.014	0.099 ± 0.011	0.092 ± 0.005
DISCoVeR (Ours)	<b>0.073 ± 0.001</b>	<b>0.083 ± 0.004</b>	<b>0.087 ± 0.002</b>	<b>0.087 ± 0.001</b>

Supplementary Table 3: Model performances on the CelebA-Glasses dataset. Bold denotes best performance.

	$I(z; w) ↓$	NLL (↓)
CSVAE - No Adv.	0.048 ± 0.014	137.522 ± 0.155
CSVAE	0.079 ± 0.029	145.989 ± 0.336
HCSVAE - No Adv.	0.055 ± 0.012	131.813 ± 0.21
HCSVAE	0.055 ± 0.014	137.319 ± 0.265
DIVA	0.188 ± 0.028	143.528 ± 0.02
CCVAE	0.083 ± 0.022	<b>131.764 ± 0.006</b>
DISCoVeR (Ours)	<b>0.030 ± 0.011</b>	135.677 ± 0.007
DISCoVeR - Common (Ours)	—	374.114 ± 0.05

## E Implementation Details

### E.1 Considerations and reproducibility

We run all experiments on a single H100 GPU. Reported means and standard deviations for tables are conducted over 10 repetitions of the experiment with different random seeds. All models are trained using the AdamW [42] optimizer until validation loss stops decreasing for 50 epochs. Wherever provided, we use mutual information neural estimation (MINE, Belghazi et al. [5]) to obtain mutual information estimates. For Naive Bayes classifiers, we use the implementation provided by *scikit-learn* [53]. To use ideal hyperparameters for each method, we consult the original implementation whenever possible, and conduct a simple grid-search to produce originally described model behavior. Implementations of all methods compared in this study, including DISCoVeR, as well as code to reproduce our results, can be found at <https://github.com/Computational-Morphogenomics-Group/DISCOVeR>. Models compared in the study admit a weighting term for each term in the loss function, of which most are shared across different approaches. We use the following shorthands for each of the terms:

$$\text{Rec.} \rightarrow \mathbb{E}_{q_{z|x}} [\mathbb{E}_{q_{w|x,y}} [\log p(x | z, w)]]$$

$$\text{D}_{\text{KL}}(Z) \rightarrow \text{D}_{\text{KL}}(q_{z|x} \| p_z)$$

$$\text{D}_{\text{KL}}(W) \rightarrow \text{D}_{\text{KL}}(q_{w|x,y} \| p_{w|y})$$

$$\text{Adv.} \rightarrow -\mathbb{E}_{q_{z|x}} [\log g(y | z)]$$

$$\text{Class.} \rightarrow \mathbb{E}_{q_{w|x,y}} [\log q(y | w)]$$

$$\text{Rec.} - (Z) \rightarrow \mathbb{E}_{q_{z|x}} [\log p(x | z)]$$

Below, we provide additional details for the hyperparameters used in each experiment, and any other external resources used to obtain the corresponding sections' results.

### E.1.1 Parametric Model

For the parametric model, we consider  $z, w \in \mathbb{R}$  and use multi-layer perceptrons (MLPs) with  $n_{hidden} = 2, d_{hidden} = 8$  to parameterize approximate posteriors, the generative model and classifiers. For all models, we use learning rate  $\gamma = 0.001$ . A more detailed table of model-specific loss weights is provided in Supplementary Table 4.

Supplementary Table 4: Loss weights for the parametric model experiment.

	Rec.	$D_{KL}(Z)$	$D_{KL}(W)$	Adv.	Class.	Rec. - ( $Z$ )
CSVAE - No Adv.	1	1	1	—	—	—
CSVAE	2.5	1	0.5	20	—	—
HCSVAE - No Adv.	1	1	0.5	—	—	—
HCSVAE	2.5	1	0.5	20	—	—
DIVA	1	1	1	—	1	—
CCVAE	1	1	1	—	1	—
DISCoVeR (Ours)	0.7	0.7	0.2	0.8	—	0.3

Supplementary Table 5: K-Means NMI for embeddings across stimulation ( $y$ ) and cell type (common structure).

	$w$ - Stimulation ( $\uparrow$ )	$z$ - Cell Type ( $\uparrow$ )	$z$ - Stimulation ( $\downarrow$ )
CSVAE - No Adv.	0.949 $\pm$ 0.003	0.702 $\pm$ 0.015	0.187 $\pm$ 0.0
CSVAE	0.939 $\pm$ 0.002	0.406 $\pm$ 0.001	<b>0.002 <math>\pm</math> 0.0</b>
HCSVAE - No Adv.	0.933 $\pm$ 0.006	0.628 $\pm$ 0.016	0.091 $\pm$ 0.002
HCSVAE	0.931 $\pm$ 0.005	0.433 $\pm$ 0.001	0.003 $\pm$ 0.0
DIVA	0.801 $\pm$ 0.0	0.628 $\pm$ 0.011	0.056 $\pm$ 0.0
CCVAE	0.604 $\pm$ 0.0	0.683 $\pm$ 0.016	0.103 $\pm$ 0.0
DISCoVeR (Ours)	<b>0.946 <math>\pm</math> 0.002</b>	<b>0.688 <math>\pm</math> 0.0</b>	<b>0.002 <math>\pm</math> 0.0</b>

### E.1.2 Noisy Swiss Roll

For this experiment, we consider  $z, w \in \mathbb{R}^2$  and use MLPs with  $n_{hidden} = 2, d_{hidden} = 128$  to parameterize approximate posteriors, the generative model and classifiers. For all models, we use learning rate  $\gamma = 0.001$ . A more detailed table of model-specific hyperparameters is provided in Supplementary Table 6.

Supplementary Table 6: Loss weights for the noisy Swiss roll experiment.

	Rec.	$D_{KL}(Z)$	$D_{KL}(W)$	Adv.	Class.	Rec. - ( $Z$ )
CSVAE - No Adv.	20	0.2	1	—	—	—
CSVAE	20	0.2	1	50	—	—
HCSVAE - No Adv.	20	0.2	1	—	—	—
HCSVAE	20	0.5	1	50	—	—
DIVA	20	0.2	0.2	—	1	—
CCVAE	20	0.2	0.2	—	1	—
DISCoVeR (Ours)	0.9	0.2	0.2	8	—	0.1

### E.1.3 Noisy Colored MNIST

For this experiment, we consider  $z \in \mathbb{R}^{20}, w \in \mathbb{R}^2$  and use convolutional neural networks (CNNs) to parameterize approximate posteriors and the generative model. For this example, DISCoVeR

can support  $z, w$  with different sizes, by parameterizing  $p(w | y)$  through neural networks. For all models, we use learning rate  $\gamma = 0.0001$ . We detail the architectures and model-specific hyperparameters in Supplementary Tables 7 - 10. All other neural networks are formulated as MLPs with  $n_{hidden} = 2, d_{hidden} = 4096$ .

Supplementary Table 7: Image encoder architecture for noisy colored MNIST. Parameters for Conv2d are input / output channels. Parameters for MaxPool2D are kernel size and stride. Parameter for the linear layer is the output size. For variances, outputs are passed through an additional Softplus layer to ensure non-negativity.

Block	Details
1	Conv2d(3,32) + BatchNorm2D + ReLU
2	Conv2d(32,32) + BatchNorm2D + ReLU + MaxPool2D(2,2)
3	Conv2d(32,64) + BatchNorm2D + ReLU + MaxPool2D(2,2)
4	Conv2d(64,128) + BatchNorm2D + ReLU + MaxPool2D(2,2)
5	Linear(4096) + BatchNorm1D + ReLU
6	Linear(4096) + BatchNorm1D + ReLU
7	Linear( $d_{latent}$ )

Supplementary Table 8: Image decoder architecture for noisy colored MNIST. Parameters for Conv2d are input / output channels. Parameters for MaxPool2D are kernel size and stride. Parameter for the linear layer is the output size.

Block	Details
1	Linear(4096) + BatchNorm1D + ReLU
2	Linear(4096) + BatchNorm1D + ReLU
3	Linear(1152) + Unflatten
4	Upsample(2) + Conv2d(128, 64) + BatchNorm2D + ReLU
5	Upsample(2) + Conv2d(64, 32) + BatchNorm2D + ReLU
6	Upsample(2) + Conv2d(32, 32) + BatchNorm2D + ReLU
7	Conv2d(32, 3) + Sigmoid

Supplementary Table 9: Latent classifier architecture for noisy colored MNIST. Outputs parameterize logits of class probabilities.

Block	Details
1	Linear(4096) + BatchNorm1D + ReLU
2	Linear(4096) + BatchNorm1D + ReLU
3	Linear(2)

Supplementary Table 10: Loss weights for the noisy colored MNIST experiment.

	Rec.	$D_{\text{KL}}(Z)$	$D_{\text{KL}}(W)$	Adv.	Class.	Rec. - ( $Z$ )
CSVAE - No Adv.	1	0.0001	1	—	—	—
CSVAE	1	0.0001	1	1	—	—
HCSVAE - No Adv.	1000	0.0001	1	—	—	—
HCSVAE	10000	0.0001	1	1	—	—
DIVA	1	0.0001	0.0001	—	1	—
CCVAE	1	0.0001	0.0001	—	1	—
DISCoVeR (Ours)	0.5	0.0001	0.0001	0.1	—	0.5

#### E.1.4 CelebA-Glasses

Motivated by the previous application of Klys et al. [32], our choices follow those outlined in Larsen et al. [36]. We provide a detailed table of model-specific hyperparameters in Supplementary Table 11:

Supplementary Table 11: Loss weights for the CelebA-Glasses experiment.

	Rec.	$D_{\text{KL}}(Z)$	$D_{\text{KL}}(W)$	Adv.	Class.	Rec. - ( $Z$ )
CSVAE - No Adv.	1	0.0001	1	—	—	—
CSVAE	1000	0.0001	1	1	—	—
HCSVAE - No Adv.	1000	0.0001	1	—	—	—
HCSVAE	10000	0.0001	1	1	—	—
DIVA	100000	0.0001	0.0001	—	1	—
CCVAE	100000	0.0001	0.0001	—	1	—
DISCoVeR (Ours)	1000000	0.0001	0.0001	2000	—	100000

#### E.1.5 scRNA-Seq

Following on the previous applications by Lopez et al. [41], we use  $z \in \mathbb{R}^{10}$ ,  $w \in \mathbb{R}^2$ . For DISCoVeR we match the dimensions and use  $w \in \mathbb{R}^{10}$  to avoid parameterizing the prior  $p(w | z, y)$  with an additional neural network. We use MLPs with  $n_{\text{hidden}} = 1$ ,  $d_{\text{hidden}} = 128$  to parameterize approximate posteriors, the generative model and classifiers. We calculate K-Means NMI through *scikit-learn* [53] by calling the `normalized_mutual_info_score` function with the original labels and the clusterings obtained by running KMeans on (1) the entire latent embedding and (2) single dimensions of the embedding and report the highest score. A more detailed table of model-specific hyperparameters is provided in Supplementary Table 12:

Supplementary Table 12: Loss weights for the scRNA-seq experiment.

	Rec.	$D_{\text{KL}}(Z)$	$D_{\text{KL}}(W)$	Adv.	Class.	Rec. - ( $Z$ )
CSVAE - No Adv.	1	0.0001	1	—	—	—
CSVAE	1	0.0001	1	100	—	—
HCSVAE - No Adv.	1	0.0001	1	—	—	—
HCSVAE	1	0.0001	1	100	—	—
DIVA	1	0.0001	0.0001	—	1	—
CCVAE	1	0.0001	0.0001	—	1	—
DISCoVeR (Ours)	0.9	0.0001	0.0001	100	—	0.1

## E.2 Summary of the scVI generative model for 5.2.3

Given batch key  $b$  and  $G$  genes, the generative model of scVI for a single cell  $x_i \in \mathbb{N}^G$  is formulated as:

$$\begin{aligned}z_i &\sim \mathcal{N}(0, 1) \\ \rho_i &= f_\theta(z_i, b_i) \\ \pi_{ig} &= h_\phi^g(z_i, b_i) \\ x_{ig} &\sim \text{ZINB}(l_i \rho_i, \theta_g, \pi_{ig})\end{aligned}$$

Here,  $g$  indexes genes,  $l_i = \sum_g x_{ig}$  denotes the total number of counts for a single cell,  $z_i$  denotes the latent representation of the cell, and  $\rho_i$  denotes the normalized expression of the cell.  $f_\theta$  is formulated as a neural network with a final softmax layer.  $h_\phi$  is a neural network used to parameterize zero-inflation probabilities for the generative zero-inflated negative binomial (ZINB) distribution. As such, for a single batch, the formulation of scVI is equivalent to the VAE with a ZINB likelihood. While all other models can be extended easily, DISCoVeR requires reconstructions as a proxy for the adversarial loss. For this formulation, we directly treat the normalized expressions  $\rho_i$  as the adversarial reconstructions  $\hat{x}$ .